Calculating the Band Structure of Photonic Crystals Through the Meshless Local Petrov-Galerkin (MLPG) Method and Periodic Shape Functions

Williams Nicomedes[1], Renato Mesquita[2], and Fernando Moreira[1]

[1]Dept. of Electronic Engineering, Federal University of Minas Gerais, Belo Horizonte, MG 31270-901, Brazil
[2]Dept. of Electrical Engineering, Federal University of Minas Gerais, Belo Horizonte, MG 31270-901, Brazil

This paper illustrates how to determine the bandgap structure of photonic crystals through MLPG. This method is akin to the Finite Element Method (FEM), as it also deals with the discretization of weak forms and produces sparse global matrices. The major difference is the complete absence of any kind of mesh. We concentrate in a particular version of it, the MLPG4, also known as Local Boundary Integral Equation Method (LBIE). Since the boundary conditions governing the electromagnetic field are periodic in a unit cell, we develop a special scheme to embed this feature on the shape functions used in the discretization process. As a result, boundary conditions do not need to be imposed on the unit cell.

***Index Terms*—Electromagnetic wave propagation, finite element methods, integral equations, photonic crystals.**

I. Introduction

MESHLESS (or meshfree) methods are a paradigm for finding numerical solutions to differential equations defined in geometrical domains without resorting to a mesh (like FEM) or to a grid (like finite-difference methods). In Electromagnetics there have been such appearances [1], where a meshless method called Element-Free Galerkin (EFG) is employed. MLPG, the particular method investigated in this paper, differs somehow from the other methods. It is peculiar in the sense that the numerical integrations are carried out in certain local domains, thus dismissing any sort of background cells [2]. Besides that, MLPG employs two kinds of functions, *shape* and *test functions*, which belong to two different spaces. The shape functions are constructed numerically, whereas there are many choices available to the test functions. As for the latter, we took the solution to Green's problem for Laplace's equation, which leads to MLPG4, or LBIE [2].

Recently, MLPG has been applied to situations in 2D electromagnetic wave propagation [3] and in 3D electrostatics [4]. We now look for applications of MLPG4 to eigenvalue problems, specifically those arising in the analysis of 2D photonic bandgap crystals. After some discussion on periodic shape functions, we present a pair of examples concerning the band structure for the TM^z polarization. The results are compared to those in [5] and [6], which solve the same problems by other methods.

II. Meshless Methods: Overview and Shape Functions

Let Ω be a two-dimensional domain (global boundary $\partial\Omega$). In order to find a numerical approximation u^h for a function u, we begin by spreading nodes across Ω. To each node is ascribed an index, i.e., a natural number $i \in \mathbb{N}$. The next step is to define shape functions associated to each node. They do not present analytical expressions; a shape function ϕ_i usually depends on the relative positions of neighboring nodes. Furthermore, they are compactly supported, i.e., different from zero only at a small region surrounding the node (called the node's *influence domain* Λ). So, given a point $\vec{x}$, there follows:

$$u(\vec{x}) \sim u^h\vec{x} = \sum_{t=1}^{N} \phi_i(\vec{x})\hat{u}_i = \mathbf{\Phi}(x)\hat{\boldsymbol{u}} \tag{1}$$

where the global index i runs through all nodes whose influence domains include point $\vec{x}$ and each $\hat{u}_i$ is the nodal parameter (a coefficient to be determined).

There are many ways in which the shape functions can be constructed. In this work, a procedure called Moving Least Squares (MLS) has been employed [7]. Given a point $\vec{x}$ at which the shape functions are to be calculated, one first finds all neighboring nodes which extend their influence domains until $\vec{x}$ (e.g., four nodes with global indices 3, 5, 10 and 18). Then one feeds this information to a numerical procedure [4] which returns the shape functions and their derivatives calculated at $\vec{x}$:

$$\begin{bmatrix} \mathbf{\Phi}(\vec{x}) \\ \partial\mathbf{\Phi}(\vec{x}) \end{bmatrix} = \begin{bmatrix} \phi_3(\vec{x}), \phi_5(\vec{x}), \phi_{10}(\vec{x}), \phi_{18}(\vec{x}) \\ \partial\phi_3(\vec{x}), \partial\phi_5(\vec{x}), \partial\phi_{10}(\vec{x}), \partial\phi_{18}(\vec{x}) \end{bmatrix} \tag{2}$$

where ∂ denotes the derivatives with respect to x or y, $\phi_3(\vec{x})$ is the shape function associated to node 3 (located at $\vec{x}_3$) calculated at $\vec{x}$, and so on.

III. Calculating the Band Structure of a Photonic Crystal: The MLPG Method

In LBIE, to each node i at $\vec{x}_i$ is ascribed a test function v_i, in addition to a shape function ϕ_i [4]. This test function acts in a specific region surrounding the node, the *test domain* Υ_i. In LBIE, Υ_i is required to be a *circle* centered at each node. Conditions on v_i are $\nabla^2 v_i(\vec{x}) = -\delta(\vec{x} - \vec{x}_i)$ (a Dirac delta at $\vec{x}_i$) and $v_i(\vec{x}) = 0$ at the boundary of the test domain, i.e., $\partial\Upsilon_i$. A function v_i satisfying the above requirements is given by $v_i(\vec{x}) = (1/2\pi)\ln(s_i/\|\vec{x} - \vec{x}_i\|)$. In this work, the radii of all test (s_i) and influence (r_i) domains are equal.

A two-dimensional photonic bandgap crystal is a periodic array of dielectric structures, one of the most remarkable properties of which is that it is able to select what wavelengths

Manuscript received July 07, 2011; revised October 26, 2011; accepted October 27, 2011. Date of current version January 25, 2012.. Corresponding author: W. L. Nicomedes (e-mail: wlnicomedes@yahoo.com.br).

Color versions of one or more of the figures in this paper are available online at http://ieeexplore.ieee.org.

Digital Object Identifier 10.1109/TMAG.2011.2175206

0018-9464/$31.00 © 2012 IEEE

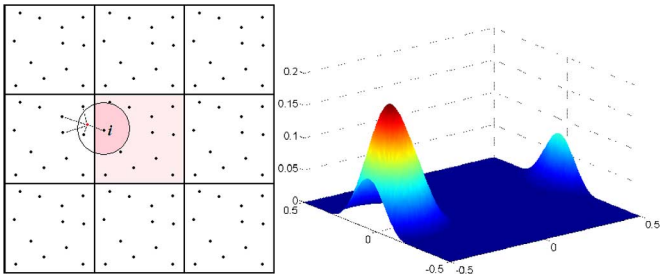

Fig. 1. *Left*: The extended domain Ω^e formed by replicating the unit cell (shaded). A node i and its test domain Υ_i, in which it is illustrated a quadrature point. Five nodes are able to influence it. *Right*: A periodic shape function in $\Omega = [-0.5, 0.5] \times [-0.5, 0.5]$, in which the equality of profiles at the left and right edges can be verified.

can actually propagate through it. A *unit cell* is a pattern that is replicated throughout the space in order to generate the crystal. In this work, we restrict our analysis to square cells (whose sides are normalized to $\bar{a} = 1$). The mathematical analysis is usually reduced to a single cell, which coincides with our computational domain Ω. For an incoming TM^z wave, the problem is modeled by the Helmholtz equation for the electric field E_z and Bloch-periodic boundary conditions [8]. However, according to Bloch's theorem, the electric field E_z can be written as $E_z(\vec{x}) = e^{-j\vec{K}\cdot\vec{x}}u(\vec{x})$, where u is now a periodic function in Ω and $\vec{K}$ is the Bloch vector. Substituting this new form for E_z in Helmholtz equation we get an equivalent problem:

$$-\nabla^2 u + j2\vec{K}\cdot\vec{K}u = (w/c)^2\varepsilon_r(\vec{x})u, \quad \vec{x}\in\Omega \tag{3}$$

$$u(\vec{x}+\vec{L}) = u(\vec{x}) \quad \partial u(\vec{x}+\vec{L})/\partial n = \partial u(\vec{x})/\partial n, \quad \vec{x}\in\partial\Omega \tag{4}$$

where ω is the angular frequency, c is the speed of light and ε_r is the relative permittivity. Boundary conditions (4) tell us that the function u (and its normal derivative) at one side of $\partial\Omega$ is equal to u at the opposite side ($\vec{L}$ is the lattice translation vector). So u is periodic in a unit cell Ω.

Given a unit cell Ω, we set up a nodal distribution on it. We then surround this cell with other 8 cells, and in each one of these extra cells, we assume a nodal distribution *identical* to that set up in Ω (i.e., we replicate it throughout). The situation is depicted in Fig. 1. This array of nine cells form an extended domain Ω^e, in the middle of which our original cell is located. We then proceed to ascribe a global index i to each one of the nodes in Ω^e. If there are, say, $N = 100$ nodes in the original cell Ω, then in Ω^e the nodes in the first cell (top left) vary from 1 to 100; in the second cell (top middle), from 101 to 200, in the third (top right), from 201 to 300, and so on. These extra nodes are used only when calculating the shape functions; as far as (3) is concerned, only Ω and its nodes are considered.

Now in order to produce the periodic shape functions, nodes that occupy the same position within each cell throughout the 9 cells are considered equivalent, e.g. nodes 2 (top left cell), 102 (top middle cell), 202 (top right cell), and so on, are all equivalent to each other. As a result of the equivalence, each node in the extended domain Ω^e can be mapped to a node inside Ω. This is carried out through another indexing scheme: $i = h(i)$, where i is a node's global index in $\Omega^e (1 \le i \le 9N)$, N is the number of nodes inside a cell, and i is the node's *generalized index* in the innermost cell $\Omega (1 \le i \le N)$. It can be proved (Section IV) that dealing with generalized indices leads to periodic shape functions in Ω. A combination of periodic shape functions is also periodic, so we can just employ them to discretize (3) and let go of the boundary conditions (4).

For each node (labeled by its generalized index i) in the innermost cell Ω, we take (3) together with $\nabla^2 v_i(\vec{x}) = -\delta(\vec{x}-\vec{x}_i)$ and insert into Green's second identity for scalar fields. The integrals are to be considered in the test domain Υ_i:

$$u(\vec{x}_i) + \oint_{\partial Y_i} u\frac{\partial v_i}{\partial n}dl + \int\!\!\int_{Y_i} (j2\vec{K}\cdot\nabla u + \vec{K}\cdot\vec{K}u)v_i dA = \left(\frac{\omega}{c}\right)^2 \int\!\!\int_{Y_i} \varepsilon_r u v_i dA. \tag{5}$$

Instead of Green's identity, one could also have applied the weighted residual method, thus getting a slightly different weak form, in which the first two terms of (5) are substituted by an area integral involving $\nabla u\cdot\nabla v_i$. Whenever u (or its derivatives) appear in (5), it is substituted by the sum of shape functions (1). For each i, we get a set of equations similar to (5), in each one of which u is replaced by a shape function ϕ_j. Moreover, these equations come multiplied by the nodal parameter $\hat{u}_j$. After this procedure is carried out for all nodes in the unit cell Ω, we get a generalized eigenvector problem of the type $\boldsymbol{R}\hat{\boldsymbol{u}} = \beta\boldsymbol{T}\hat{\boldsymbol{u}}$, which is easily solved for the eigenvalues $\beta = (\omega/c)^2$. $\boldsymbol{R}$ and $\boldsymbol{T}$ are $N \times N$ sparse matrices.

The weak forms must be integrated numerically (Gaussian quadratures). In filling up the matrix $\boldsymbol{R}$, we consider the area (and contour) integral in the left of (5). First, we take a node i in Ω and spread a set of quadrature points $\vec{x}_g$ throughout Υ_i (and $\partial\Upsilon_i$). Second, we determine which nodes from the extended domain Ω^e influence each $\vec{x}_g$ (it does not matter $\vec{x}_g$ if lies outside Ω, like in Fig. 1). Third, from the nodes $\{a, b, \ldots, n\}$ taken from the total of $9N$ we determine their generalized indices $\{h(a), h(b), \ldots, h(n)\}$. At last, we add the contribution of node a to the element $(i, h(a))$ in the matrix $\boldsymbol{R}$, and so on for the other contributing nodes. This is repeated for all quadrature points. The integral in the right of (5) is treated likewise, which leads to the matrix $\boldsymbol{T}$.

IV. Exploring the Periodic Shape Functions

In this section we give a formal proof of why appealing to generalized indices produces periodic shape functions in a cell Ω. Some propositions and definitions are necessary:

(***p1***) I is a set of natural numbers: $I = \{i \in \mathbb{N} | 1 \le i \le 9N\}$. These numbers are the indices of the nodes in Ω^e.

(***p2***) R is an equivalence relation on I given by: $R = \{(i,j) \in I \times I | \exists k \in \mathbb{Z}(i - j = kN)\}$. For an arbitrary number $i \in I$, $i - i = 0 = 0N$, so $(i,i) \in R$. Therefore R is reflexive. For an arbitrary member $(i,j) \in R$, $i - j = kN$ for some $k \in \mathbb{Z}$. Consequently, $j - i = -kN$. However, $-k \in \mathbb{Z}$, and hence $(j,i) \in R$. So R is symmetric. If two arbitrary members $(i,j) \in R$ and $(j,m) \in R$, so $i - j = k_1 N$ and $j - m = k_2 N$ for some $k_1, k_2 \in \mathbb{Z}$. It follows that $i - m = (k_1 + k_2)N$, and since $k_1 + k_2 \in \mathbb{Z}$,

$(i,m) \in R$. So R is transitive. R is reflexive, symmetric and transitive; hence R is an equivalence relation.

(***p3***) S is a relation on $\mathbb{R}^2 : S = \{((x,y),(x',y')) \in \mathbb{R}^2 \times \mathbb{R}^2 | \exists m \in \mathbb{Z} \exists n \in \mathbb{Z}(x - x' = m\bar{a} \text{ and } y - y' = n\bar{a})\}$. The pair $(\vec{x},\vec{x}') \in S$ if both the horizontal and vertical components of the vector joining them are multiples of the unit cell length $\bar{a}$.

(***d1***) $f : I \to \mathbb{R}^2$ is a function such that $f(i) = (x_i, y_i)$. The function f ascribes an index to a node located at a point (x,y) in Ω^e.

(***d2***) $g_{mn} : \mathbb{R}^2 \to \mathbb{R}^2$ is a translation function: $g_{mn}(\vec{x}) = g_{mn}(x,y) = (x + m\bar{a}, y + n\bar{a}) = \vec{x}'$. The function g_{mn} takes a point $\vec{x}$ to another point $\vec{x}'$ such that $(\vec{x},\vec{x}') \in S$.

(***p4***) Let us suppose that

$$\forall \vec{x} \in \mathbb{R}^2 \, (\exists i \in I \, (\vec{x} = f(i)) \to \forall \vec{x}' \in \mathbb{R}^2 \, ((\vec{x},\vec{x}') \in S \to \exists j \in I \, (\vec{x}' = f(j))))$$

i.e., if there is a node with index i located at $\vec{x}$, then if $\vec{x}'$ is such that $(\vec{x},\vec{x}') \in S$, so there is another node with index j located at $\vec{x}'$. Replicating the unit cell in the aforementioned process of constructing Ω^e guarantees this.

(***p5***) Suppose $\forall i \in I \forall j \in I((f(i),f(j)) \in S \to (i,j) \in R)$. i.e., if the components of the vector joining two nodes are multiples of a, then their indices differ by an integer multiple of N. This is assured through the process of consecutively numbering the nodes in the process of constructing Ω^e.

(***d3***) Let $h : I \to \{1,\ldots,N\}$ be such that $h(i) = \min[i]_R$. Since R is an equivalence relation, R breaks the set I into partitions, i.e., the *equivalence classes* $[i]_R$, where $[i]_R = \{j \in I | (j,i) \in R$. Each node i in I belongs to only one equivalence class iR, e.g., if $N = 100$, then $[2]_R = \{2, 102, \ldots, 802\}$. Clearly there are N equivalence classes, each one containing nine members. The generalized index mentioned earlier is just a representative for each equivalence class, taken to be its smallest element: $i = h(i) = \min[i]_R$.

(***p6***) MLS shape functions (and their derivatives) are invariant under translations. We illustrate this through a picture. Suppose that five nodes at the vertices of a pentagon $(\vec{x}_1,\ldots,\vec{x}_5)$ influence a point $\vec{x}$ located at its center. The contributions are given by $([\phi_1(\vec{x}),\ldots,\phi_5(\vec{x})]([\partial\phi_1(\vec{x}),\ldots,\partial\phi_5(\vec{x})])$. If we translate this pentagon some distance away from the first, the contributions of the nodes located at $\vec{x}'_1,\ldots,\vec{x}'_5$ calculated at the center $\vec{x}'$ of the new pentagon will be exactly the same as before the translation.

We now proceed to state the periodicity condition of the shape functions, in what concerns the left and right edges of a cell (the top and bottom edges are treated likewise, by substituting the translation function g_{01} for g_{10}).

Proposition(*): Periodicity of Shape Functions: Let i be a generalized index. If two points $\vec{x}$ and $\vec{x}'$ are such that $\vec{x}' = g_{10}(\vec{x})$, then $\phi_i(\vec{x}) = \phi_i(\vec{x}')$.

To prove it, we need a lemma regarding equivalence classes:

Lemma 1: Let α and β be elements of I. If $\beta \in [\alpha]_R$, then $[\beta]_R = [\alpha]_R$.

Proof of Lemma 1: Let γ be an arbitrary element of $[\beta]_R$. So $(\gamma,\beta) \in R$. Since $\beta \in [\alpha]_R$, $(\beta,\alpha) \in R$. But R is transitive, and then $(\gamma,\alpha) \in R$ or $\gamma \in [\alpha]_R$. Since γ was arbitrary, $[\beta]_R \subset [\alpha]_R$. Now let δ be an arbitrary element of $[\alpha]_R$. So $(\delta,\alpha) \in R$. Since $\beta \in [\alpha]_R$, $(\beta,\alpha) \in R$. But R is symmetric, so $(\alpha,\beta) \in R$. As $(\delta,\alpha) \in R$ and $(\alpha,\beta) \in R$, and by the transitivity of R we conclude that $(\delta,\beta) \in R$, or $\delta \in [\beta]_R$. Since δ was arbitrary, $[\alpha]_R \subset [\beta]_R$. From $[\alpha]_R \subset [\beta]_R$ and $[\beta]_R \subset [\alpha]_R$, $[\alpha]_R = [\beta]_R$. ■

Proof of (*): Let i be a generalized index. Suppose that $\vec{x}$ and $\vec{x}'$ are arbitrary points such that $\vec{x}' = g_{10}(\vec{x})$ (e.g., $\vec{x}$ is in the left edge and $\vec{x}'$ in the right edge). Let $\{\vec{y}_1 \ldots, \vec{y}_n\}$ be the set of n nodes influencing $\vec{x}$. Since they are nodes, they are labeled by indices, i.e., $\vec{y}_k = f(\alpha_k), 1, \ldots, k, \ldots, n$. As each $\vec{y}_k \in \mathbb{R}^2$ and has an associated index α_k, (***p4***) tells us that $\forall \vec{t}' \in \mathbb{R}^2((\vec{y}_k,\vec{t}') \in S \to \exists j \in I(\vec{t}' = f(j)))$. However, if for each $\vec{y}_k$ we take a point $\vec{t}' = \vec{z}_k = g_{10}(\vec{y}_k)$, we clearly verify that $(\vec{y}_k,\vec{z}_k) \in S$. So by (***p4***) there is a node at $\vec{z}_k$, whose index is $j = \beta_k$ such that $\vec{z}_k = f(\beta_k)$. This picture reveals us that there is a set of nodes $\{\vec{z}_1,\ldots,\vec{z}_n\}$ that could be obtained by a translation g_{10} of the nodes in $\{\vec{y}_1,\ldots,\vec{y}_n\}$. Because $\vec{x}'$ has also been obtained by a translation g_{10}, (***p6***) says that $\phi_{\alpha_1}(\vec{x}) = \phi_{\beta_1}(\vec{x}'),\ldots,\phi_{\alpha_n}(\vec{x}) = \phi_{\beta_n}(\vec{x}')$. Consequently, if we re-label the indices through h the function we get $\phi_{h(\alpha_1)}(\vec{x}) = \phi_{h(\beta_1)}(\vec{x}'),\ldots,\phi_{h(\alpha_n)}(\vec{x}) = \phi_{h(\beta_n)}(\vec{x}')$. By (***p5***), since $(\vec{y}_1,\vec{z}_1) \in S,\ldots,(\vec{y}_n,\vec{z}_n) \in S$, then $(\alpha_1,\beta_1) \in R,\ldots,(\alpha_n,\beta_n) \in R$. So $\alpha_1 \in [\beta_1]_R,\ldots\alpha_n \in [\beta_n]_R$. But according to lemma 1, $[\alpha_1]_R = [\beta_1]_R,\ldots,[\alpha_n]_R = [\beta_n]_R$. So $h(\beta_k) = \min[\beta_k]_R = \min[\alpha_k]_R = h(\alpha_k)$, $1,\ldots,k,\ldots,n$. Therefore $\phi_{h(\alpha_1)}(\vec{x}) = \phi_{h(\alpha_1)}(\vec{x}'),\ldots,\phi_{h(\alpha_n)}(\vec{x}) = \phi_{h(\alpha_n)}(\vec{x}')$. Back to the generalized index i, there are two possible cases: Case 1: $i \in \{h(\alpha_1),\ldots,h(\alpha_n)\}$. So $\phi_i(\vec{x}) = \phi_i(\vec{x}')$. Case 2: $i \notin \{h(\alpha_1),\ldots,h(\alpha_n)\}$. If i does not figure in the list of indices, then $\phi_i(\vec{x}) = \phi_i(\vec{x}') = 0$. From both exhaustive cases, we get $\phi_i(\vec{x}) = \phi_i(\vec{x}')$. The same reasoning applies for the derivatives. Since this is valid for all points $\vec{x}$ and $\vec{x}'$ such that $\vec{x}' = g_{10}(\vec{x})$ and for all generalized indices $1 \le i \le N$, the proposition concerning the periodicity of the shape functions is proved.

In order to visualize a shape function associated to a generalized index i (Fig. 1), we take a set of points $\vec{x}$ spread throughout Ω. The MLS procedure applied to each of them returns a set of indices $\{a,b,\ldots,i,\ldots\} \subset I$ indicating which nodes influence $\vec{x}$, together with the values of the shape functions evaluated at $\vec{x}$. We compute the generalized indices

$$h(i) = \min[i]_R = \begin{cases} i \bmod N, & i \neq pN, p \in \mathbb{N} \\ N, & i = pN, p \in \mathbb{N} \end{cases} \quad (6)$$

and verify if i is among them.

V. Results

The eigenvalues of (3) depend on the Bloch vector $\vec{K}$, which is unknown. In this paper, the Bloch vector varies from point $\boldsymbol{\Gamma}(\vec{K} = [0,0])$ to point $\boldsymbol{X}(\vec{K} = [\pi/a, 0])$, from $\boldsymbol{X}$ to $\boldsymbol{M}(\vec{K} = [\pi/a, \pi/a])$, and finally from $\boldsymbol{M}$ back to $\boldsymbol{\Gamma}$. The first crystal studied is an array of circular dielectric rods, with radii given by $0.2\bar{a}$ and $\varepsilon_r = 8.9$. The second crystal is a square array of dielectric veins ($\varepsilon_r = 8.9$ and thickness $0.165\bar{a}$). Fig. 2 shows

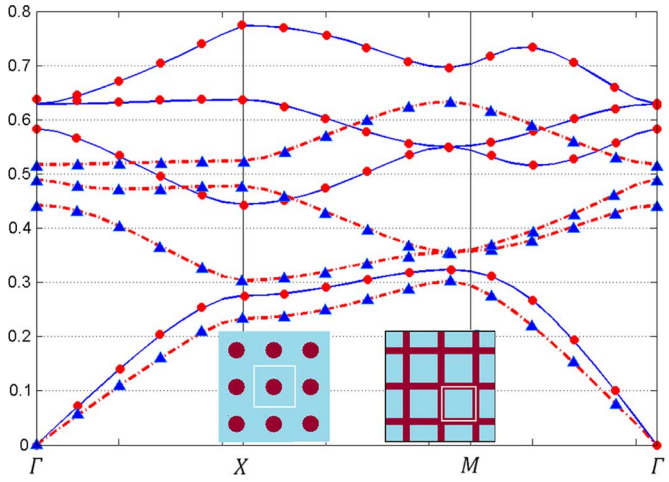

Fig. 2. The band structure for two photonic crystals (frequencies normalized to $\omega a/2\pi c$). Solid lines: MLPG results for the crystal formed by circular rods (left inset). Balls: results from [5] for this same crystal. Dashed lines: MLPG results for the dielectric veins (right inset). Triangles: results from [5] for this crystal. The unit cell is highlighted at each inset by a white square.

a very good agreement between the results of MLPG and those provided in [5] and [6]. In calculating the eigenvalues, the first problem required 625 nodes in Ω (1 DoF per node), whereas the second required 400. The area integrals in the weak forms are calculated with 128 quadrature points. Fig. 2 also reveals the existence of a bandgap around $\omega a/2\pi c = 0.4$ (for the first example); incoming waves with this frequency are unable to propagate through the crystal. To verify this, we take a large crystal and remove some rods, forming a channel (Fig. 3). Theoretically, the wave cannot leak into the bulk of the crystal, and is forced to flow along the channel. Our domain Ω is now a square around the dielectric rods. Dirichlet conditions corresponding to the incident wave e^{-jkx} are imposed in $\partial\Omega$ [8]. MLPG results (Fig. 3, now with normal shape functions, since this is a boundary-value problem) are as accurate as those provided by FEM (Fig. 4). The MLPG solution in this problem requires 3600 nodes, and the integration of the weak forms are again carried out with 128 quadrature points per test domain. This is the main drawback of MLPG, i.e., the amount of computational power used to integrate the weak forms. However, it requires fewer nodes than FEM, which used 510 000 DoF (approx. 120 000 nodes).

VI. Conclusion

In this paper we showed that MLPG can be employed as an extra tool in the analysis of photonic crystals along with FEM, PWE, RBF and FLAME [8]. The integration of weak forms in simple circular domains and the simple way of finding periodic shape functions make this method worth being given consideration in the study of photonic crystals. Future works will be directed towards other crystal geometries, and to the study of the

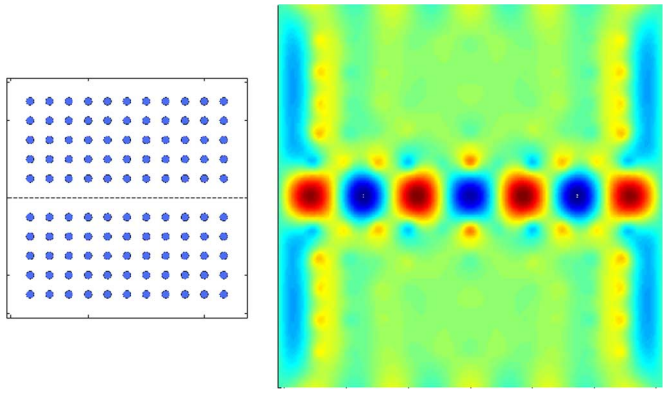

Fig. 3. *Left*: A photonic crystal formed by dielectric rods, in which a row has been removed. *Right*: Real part of the electric field throughout the domain.

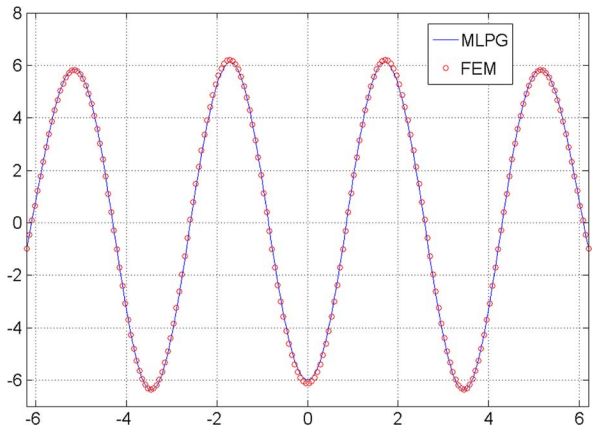

Fig. 4. A comparison between MLPG and FEM. Real part of the electric field along the dashed line indicated in the left of Fig. 3.

TE^z polarization, in which the discontinuity of normal derivatives [4] play an important role.

References

[1] A. Manzin and O. Bottauscio, "Element-free galerkin method for the analysis of electromagnetic-wave scattering," *IEEE Trans. Magn.*, vol. 44, no. 6, pp. 1366–1369, 2008.

[2] S. Atluri and S. Shen, "The meshless local Petrov-Galerkin method: A simple & less-costly alternative to the finite-element and boundary element methods," *CMES*, vol. 3, no. 1, pp. 11–51, 2002.

[3] B. C. Correa, E. J. Silva, A. R. Fonseca, D. B. Oliveira, and R. C. Mesquita, "Meshless local Petrov-Galerkin approach in solving microwave guide problems," *IEEE Trans. Magn.*, vol. 47, no. 5, pp. 1526–1529, 2011.

[4] W. Nicomedes, R. Mesquita, and F. Moreira, "A meshless local boundary integral equation method for three dimensional scalar problems," *IEEE Trans. Magn.*, vol. 47, no. 5, pp. 1214–1217, 2011.

[5] E. E. Hart, S. J. Cox, and K. Djidjeli, "Compact RBF meshless methods for photonic crystal modelling," *J. Comput. Phys.*, vol. 230, pp. 4910–4921, 2011.

[6] J. D. Joannopoulos, S. G. Johnson, J. N. Winn, and R. D. Meade, *Photonic Crystals: Molding the Flow of Light*. Princeton, NJ: Princeton Univ. Press, 2008, p. 68, p. 72.

[7] G. R. Liu, *Mesh Free Methods: Moving Beyond the Finite Element Method*, 2 ed. Boca Raton, FL: CRC Press, 2009.

[8] I. Tsukerman, *Computational Methods for Nanoscale Applications*, ser. Nanostructure Science and Technology Series. New York: Springer, 2008.